Microwave absorbing properties of multi-walled carbon nanotubes/polyaniline nanocomposites

Hua Qiu · Jin Wang · Shuhua Qi · Zheng He · Xun Fan · Yeqing Dong

Abstract Multi-walled carbon nanotubes/polyaniline (MWCNTs/PANI) nanocomposites with high absorbing properties were successfully prepared through in situ chemical polymerization. The corresponding morphologies, microstructures, thermal stabilities and microwave absorbing properties were analyzed by scanning electron microscopy, Fourier transform infrared spectroscopy, Ultraviolet–Visible spectroscopy (UV–Vis), X-ray diffraction spectroscopy, thermogravimetric analysis and vector network analyzer. Results indicated that there were strong interactions between π-bonded surface of MWCNTs and quinoid rings of PANI. In addition, the thermal stabilities and the microwave absorbing properties showed significant improvement due to the synergistic effect of MWCNTs and PANI. The reflection loss (R) of MWCNTs/PANI nanocomposites was lower than −10 dB between 8.2 and 10.2 GHz, and the minimum loss value was −49.6 dB at 8.8 GHz. The improved microwave absorbing properties suggested promising application of MWCNTs/PANI nanocomposites in high-performance microwave absorber.

1 Introduction

Conducting polymers possess lots of remarkable properties, such as light weight, corrosion resistance, good and flexible processibility and variable conductivity, and widely used in the fields of electronics [1], biomedical engineering [2–4], supercapacitors [5], energy storage [6], and so on [7]. Herein, polyaniline (PANI) has been receiving considerable attention because of its easy and inexpensive preparation, good environmental stabilities in both doped and undoped forms, excellent physical and chemical properties, and unique doping mechanism [8]. However, intrinsic low electric conductivity and low aspect ratio of the conducting polymer have restricted the application of PANI, especially as microwave absorbing materials.

Recent studies have shown that by incorporation different fillers, such as metal (Ag) [9], metal oxides (TiO$_2$ [10], ZnO [11], Fe$_3$O$_4$ [12]), carbon materials (such as CNT [13], graphite [14], carbon black [15], and graphene [16]), etc., into the PANI matrix is one of the most easy and effective way to improve the comprehensive properties of PANI matrix. Multi-walled carbon nanotubes (MWCNTs) are the suitable candidate for PANI-based nanocomposites owing to their excellent electrical and thermal conductivity, and display nonlinear optical properties and superior mechanical strength [17–22].

In our present work, MWCNTs were introduced into PANI to fabricate MWCNTs/PANI nanocomposites with high absorbing properties via in situ chemical oxidation polymerization. The corresponding morphologies, microstructures, thermal stabilities and microwave absorbing properties were investigated by scanning electron microscopy (SEM), Fourier transform infrared spectroscopy(FTIR), Ultraviolet–Visible spectroscopy (UV–Vis), X-ray diffraction spectroscopy (XRD), thermogravimetric analysis(TGA) and vector network analyzer.

2 Materials and methods

2.1 Materials

MWCNTs with a diameter in the range of 60–100 nm were purchased from Shenzhen Nanotech Port Co. Ltd.

H. Qiu (✉) · J. Wang · S. Qi · Z. He · X. Fan · Y. Dong
Department of Applied Chemistry, School of Science,
Northwestern Polytechnical University, Xi'an 710072,
People's Republic of China
e-mail: ufollowi@gmail.com

(Guangdong, China). The monomers of aniline, ammonium peroxydisulfate (APS) and sucrose stearate ester (SSE) were received from Tianjin Fuchen Chemical Reagent Factory (Tianjin, China); ethanol, acetone, nitric acid, sulfonic acid, and hydrochloric acid were of analytical grade and received from Xi'an Industry of Chemical Reagents (Shaanxi, China).

2.2 Purification and functionalization of MWCNTs

In order to effectively remove metal catalyst, metal oxide and the amorphous carbon, the purification and functionalization of MWCNTs were carried as follows. The crude MWCNTs were stirred in the mixtures of HNO_3/H_2SO_4 solution (volume ration of 3:1) and refluxed for 24 h at 105 °C. After the treatment, the samples were filtered and washed with distilled water, and then calcined at 500 °C for 1 h.

2.3 Preparation of MWCNTs/PANI nanocomposites

MWCNTs/PANI nanocomposites were synthesized via in situ polymerization of aniline using APS as the oxidant in the presence of MWCNTs. In a typical polymerization system, the solution of 1 M HCl containing 0.25 g MWCNTs and 1 g SSE was sonicated at room temperature for 24 h, then 2 g aniline monomer was added into the suspension. The mixture above was cooled down to 0 °C with mechanical stirring for 30 min. A solution of APS in water was then added dropwise within 1 h. The ultimate mixture was stirred at 0 °C for another 4 h to complete the polymerization. The resulting precipitate was filtered and rinsed with ethanol, acetone, and distilled water in sequence, in order to completely remove the oligomer. Finally, the product was dried in an oven at 60 °C for 24 h. For comparison, different amounts of MWCNTs: 0, 0.25, 0.5, 1 and 2 g, were introduced to the polymerization system, respectively, and the obtained samples were named as PANI, MWCNTs/PANI—0.25, MWCNTs/PANI—0.5, MWCNTs/PANI—1, and MWCNTs/PANI—2, respectively.

2.4 Characterizations

SEM observations of the samples were performed using a Quanta 600FEG field emission scanning electron microscope (FEI, USA). Fourier transform infrared spectroscopy (FTIR) spectra of MWCNTs/PANI sampled in KBr pallets were obtained using a WQF-510A FTIR (Rayleigh, China) with a resolution of $2 \, cm^{-1}$ in the range of $400–4,000 \, cm^{-1}$. Ultraviolet–Visible spectroscopy (UV–Vis) spectra of MWCNTs, MWCNTs/PANI and PANI were obtained with a UV-3200S Spectrophotometer (MAPADA, Shanghai) using distilled water and N-methyl-2-pyrrolotone (NMP) as solvent, respectively. The wavelength was ranged from 800 to 300 nm. X-ray diffraction patterns of samples were performed with a X'Pert MPD PRO instrument (PANalytical, Holland) for the structural characterization on powder samples from 10° to 80° at room temperature. The thermal stabilities of samples were performed using a STA 449 F3 thermogravimetric analyzer (STA 449F3, Netzschgroup, Germany) in the temperature range 40–800 °C with a heating rate of 10 °C/min under argon atmosphere.

The permittivity (ε', ε'') of samples were performed using a HP8753D vector network analyzer in the frequency range of 8.2–12.4 GHz (X-band). Powder samples were mixed with paraffin, then compressed in rectangular pellets (22.86 mm × 10.16 mm × 2.00 mm) and inserted in a copper sample holder, connected between the waveguide flanges of the network analyzer.

The microwave absorbing properties of materials can be calculated based on the complex permittivity ($\varepsilon^* = \varepsilon' - j\varepsilon''$) and complex permeability ($\mu^* = \mu' - j\mu''$). Herein, the magnetic parameters (μ', μ'') are nearly 1 and zero, respectively. The equation is as follows [23]:

$$R = 20 \log \left| \frac{Z_{in} - Z_0}{Z_{in} + Z_0} \right| \tag{1}$$

where R (dB) is the reflection loss, $Z_0 = \sqrt{\mu_0 \varepsilon_0} = 377 \, \Omega$ and Z_{in} can be described as:

$$Z_{in} = Z_0 \left(\sqrt{\frac{\mu^*}{\varepsilon^*}} \right) \tanh \left[j \left(\frac{2\pi ft}{c} \right) \left(\sqrt{\mu^* \varepsilon^*} \right) \right] \tag{2}$$

where t is the thickness of the absorber in millimeter, f is the microwave frequency in hertz, c is the velocity of light, ε^* and μ^* are complex permeability and permittivity, respectively.

3 Results and discussion

SEM images of PANI, MWCNTs and MWCNTs/PANI nanocomposites were shown in Fig. 1. It was observed that PANI nanorods were formed with diameters ranging from 87 to 176 nm (Fig. 1a), while functionalized MWCNTs was displaying a smooth surface with diameters ranging from 23 to 75 nm (Fig. 1b). When MWCNTs were introduced to the in situ aniline polymerization system, they were encapsulated by PANI (Fig. 1c), and the surfaces became rougher due to the deposition of PANI (Fig. 1d). With the increasing addition of MWCNTs, the uniformly MWCNTs/PANI nanorods were formed and the diameters became larger, increased from 124 (Fig. 1d) to 143 nm (Fig. 1e). However, further increasing addition of MWCNTs led some of the MWCNTs aggregated (marked
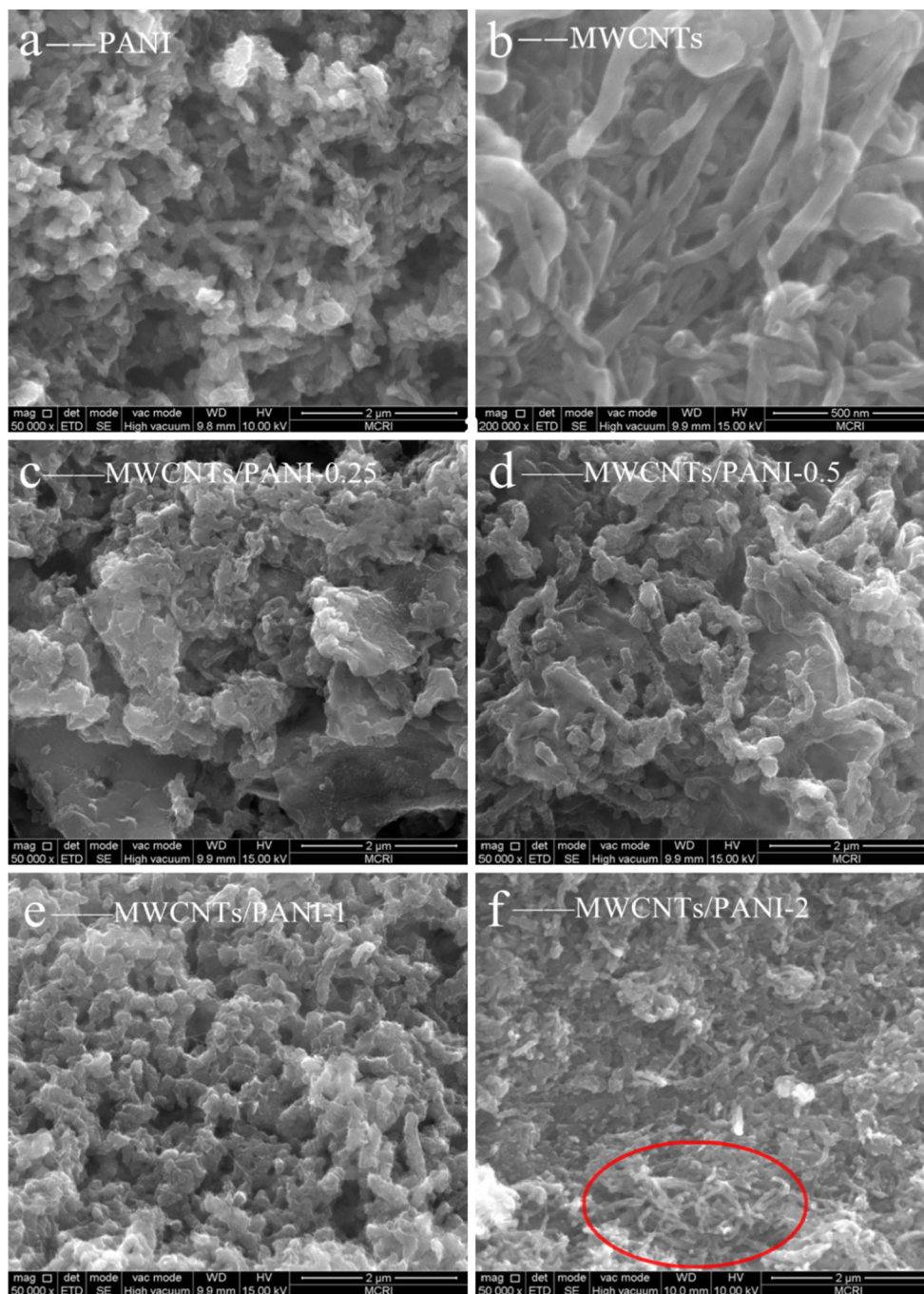
Fig. 1 SEM images of PANI, MWCNTs and MWCNTs/PANI nanocomposites

in red circle) and mixed with composites nanorods (Fig. 1f). Results showed that the composite structure of MWCNTs/PANI might lead to a high electrical conductivity due to a remarkable increase in conductive pathways.

On the basis of the analysis above, a possible formation mechanism of MWCNTs/PANI nanocomposites was proposed. In the chemical oxidation polymerization of aniline, two nucleation sites which were generated on the solid surfaces of functionalized MWCNTs (heterogeneous nucleation) and formed by aniline micelles in bulk solution (homogeneous nucleation), respectively, competed with each other [24, 25]. Active nucleation sites were generated on the surface of MWCNTs at the beginning process of polymerization and could minimize the interfacial energy barrier between the solid surface and bulk solution. Moreover, the functional groups (e.g., hydroxyl, carbonyl, and epoxy groups) of MWCNTs acted as anchor sites and
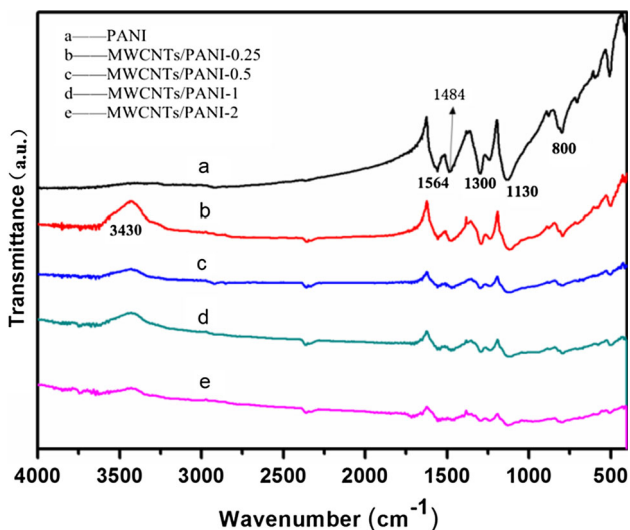
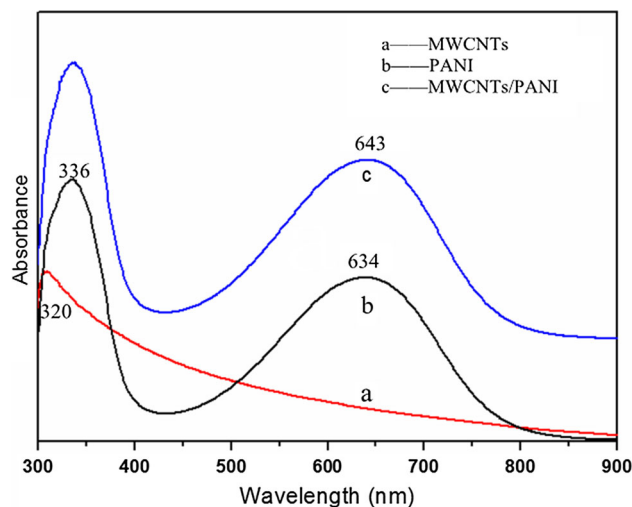**Fig. 2** FTIR spectra of PANI and MWCNTs/PANI nanocomposites

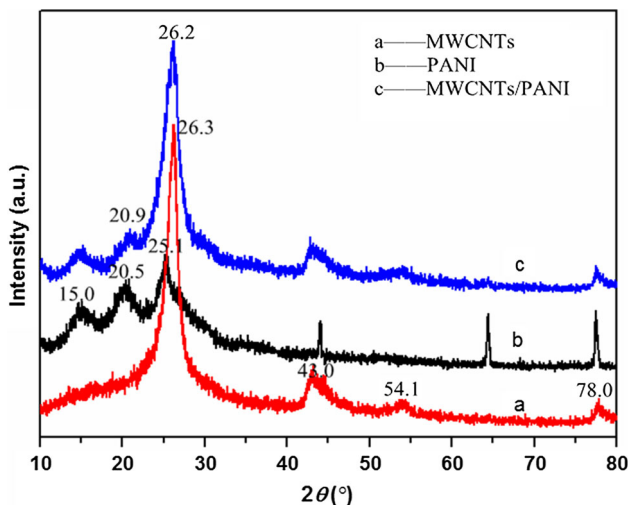**Fig. 4** UV–Vis spectra of MWCNTs, PANI, and MWCNTs/PANI nanocomposite

Fig. 3 XRD patterns of MWCNTs, PANI, and MWCNTs/PANI nanocomposite

Fig. 5 TGA curves of PANI and MWCNTs/PANI nanocomposites

facilitated the polymerization of aniline attaching on the surfaces of MWCNTs. Therefore, the heterogeneous nucleation dominated during the initial polymerization of aniline. With a small amount addition of MWCNTs, homogeneous polymerization took place after the initial nucleation on the solid surface which resulted in the aggregation of PANI. With the increasing addition of MWCNTs, after the initial nucleation on the solid surface, homogeneous nucleation was suppressed owing to the low concentration. Thus, polyaniline grew further along the initial nuclei, and MWCNTs/PANI nanorods were formed uniformly. With the further increasing addition of MWCNTs, some MWCNTs were aggregated and finally mixed with MWCNTs/PANI nanocomposites.
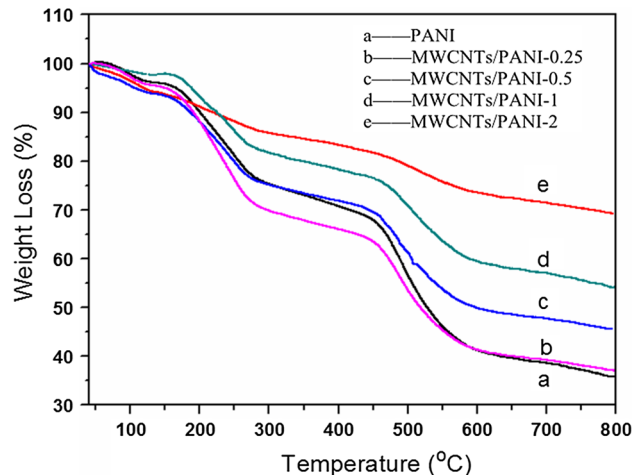
FTIR spectra for pristine PANI and MWCNTs/PANI nanocomposites were shown in Fig. 2. From Fig. 2a, the spectrum of PANI exhibited band at 794 cm^{-1} attributed to in-plane C–H bending vibrations of the benzenoid rings. The bands at 1,300 and 1,242 cm^{-1} were ascribed to C–N stretching vibrations of PANI. The bands at 1,564 and 1,486 cm^{-1} corresponded to the stretching vibrations of quinonoid and benzenoid rings, respectively. The band at 1,134 cm^{-1} was a characteristic peak of PANI conductivity, which was described as the "electric-like band" and could measure the degree of delocalization of electrons [26, 27]. Compared to the spectrum of PANI, the spectra of MWCNTs/PANI nanocomposites exhibited new bands at 3,430 cm^{-1}, which was attributed to the vibrations of

Fig. 6 Dielectric parameters and reflection loss (R) of PANI, MWCNTs and MWCNTs/PANI nanocomposite
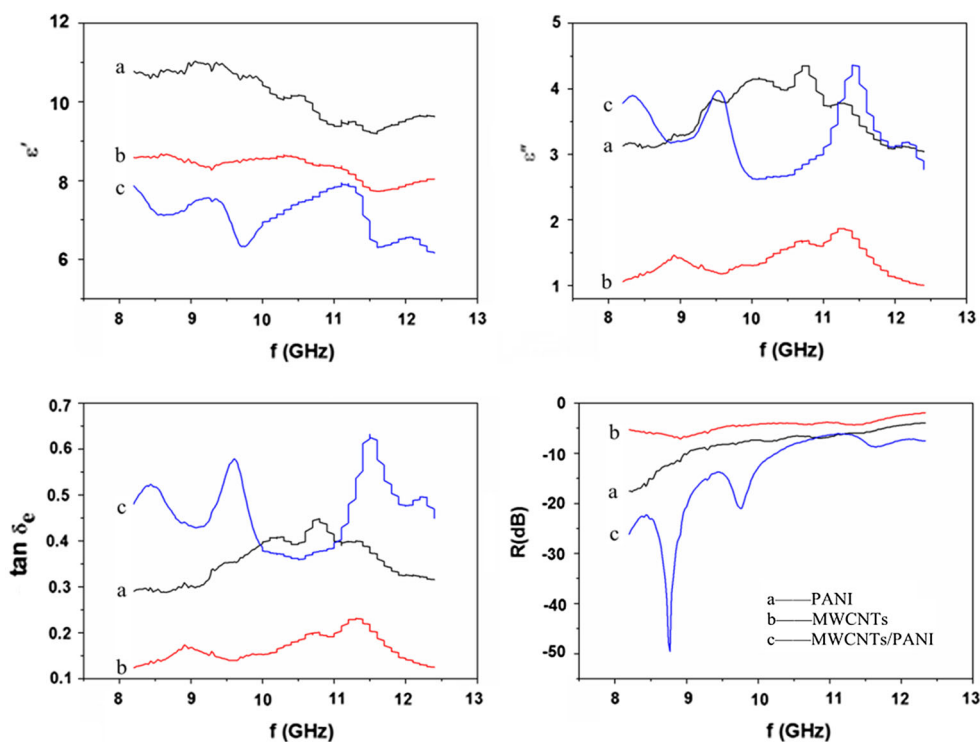
functional groups O–H. With the increasing addition of MWCNTs, the corresponding bands intensity was decreased, and the bands at 1,564 and 1,486 cm^{-1} moved toward lower wavenumbers. It suggested that the strong interactions between MWCNTs and PANI could promote and/or stabilize the quinoid and benzenoid rings, especially through the π-bonded surface of MWCNTs interacting with the conjugated structure of PANI.

The ordered structures of MWCNTs, PANI and MWCNTs/PANI composites were investigated by XRD, as shown in Fig. 3. The XRD pattern of MWCNTs displayed four peaks at 26.3°, 43.0°, 54.1° and 78.0°, which were assigned to (002), (100), (004) and (110) diffractions, respectively [28, 29]. For pure PANI, three sharp diffraction peaks at 15.0°, 20.5° and 25.1° were ascribed to (011), (020) and (200) crystal planes of PANI [30]. In the case of MWCNTs/PANI, the peaks of PANI at 20.5° and 25.1° had slightly upward shifted to 20.9° and 26.2°, respectively. The shift was attributed to an increase in the intermolecular spacing due to strong interactions between PANI and MWCNTs, finally to enhance the strong polarization effects in PANI.

The UV–Vis spectra of PANI, MWCNTs, and MWCNTs/PANI nanocomposites were shown in Fig. 4. In the case of MWCNTs with deionized water as solvent, Fig. 4a showed a characteristic peak of MWCNTs at 320 nm [31]. Two absorption bands of PANI at 336 and 634 nm were assigned to π − π* transitions in benzenoid

rings and exciton absorption of quinoid rings (n − π*) in the chain of polyaniline, respectively [32]. As MWCNTs prefigured, the spectrum of MWCNTs/PANI was similar to that of PANI. Furthermore, the absorption band at 634 nm slightly shifted to 643 nm, which indicated that the interactions between MWCNTs and PANI could promote and/or stabilize the quinoid ring structure. The π-bond surface of MWCNTs might interact strongly with the conjugated structure of PANI, especially through the quinoid rings [17], which further confirmed that PANI and MWCNTs interacted strongly through aromatic structures and the basal plane of graphitic surfaces via π-stacking.

TGA curves of PANI and MWCNTs/PANI composites were presented in Fig. 5. It could be seen that the mass loss of PANI was less than 10 % from 40 to 150 °C due to the loss of unbound water and HCl. The second obvious mass loss occurred at 150–360 °C, which was attributed to the loss of bound water and HCl, acting as secondary dopant and primary dopant, respectively. The third mass loss shown at 360–800 °C was ascribed to the decomposition of PANI. Compared to that of PANI, the mass loss of MWCNTs/PANI nanocomposites were slightly higher than that of PANI from 40 to 150 °C, which might ascribe to the higher hydrophilicity of functionalized MWCNTs. In addition, with the increasing addition of MWCNTs, the residue of MWCNTs/PANI at 800 °C was 37.1 % (b), 45.5 % (c), 54.1 % (d) and 69.2 % (e), respectively, all higher than that of PANI (35.7 %), which further illustrated

that the strong interactions between MWCNTs and PANI were beneficial to a better thermal stability of MWCNTs/PANI.

According to the absorbing mechanism, the absorbing property of materials is related to the complex permittivity ($\varepsilon^* = \varepsilon' - j\varepsilon''$), complex permeability ($\mu^* = \mu' - j\mu''$), dielectric loss (tan $\delta_e = \varepsilon''/\varepsilon'$) and magnetic loss (tan $\delta_m = \mu''/\mu'$). Since the magnetic parameter μ', μ'' was nearly 1 and zero, respectively, the absorbing properties of MWCNTs, PANI and MWCNTs/PANI were mainly attributed to the mechanism of dielectric loss [33].

On the basis of the measured data, the microwave-absorbing properties of the obtained samples were calculated and expressed by the reflection loss [21, 34].

Figure 6 showed the dielectric parameters and reflection loss of PANI, MWCNTs and MWCNTs/PANI. It was obvious that the reflection loss of MWCNTs was about −6 dB in the X band, which suggested the microwave absorbing property of single MWCNTs was not good due to its lowest ε', ε'' and tan δ_e. The reflection loss of PANI was below −10 dB (90 % absorption) at 8.2–9.0 GHz, and the minimum loss value was −17.5 dB at 8.2 GHz. Compared to that of PANI and MWCNTs, the microwave absorbing properties of MWCNTs/PANI nanocomposites showed significant improvement; the reflection loss of MWCNTs/PANI was below −10 dB at 8.2–10.2 GHz, and the minimum loss value was −49.6 dB at 8.8 GHz, higher than the reported value [33]. The enhanced microwave absorbing properties resulted from the synergetic effect of functionalized MWCNTs and in situ polymerized PANI. This mainly was attributed to the space charge polarization and decrease in carrier mobility [35]. The space charge polarization was caused by the significant difference between the electrical conductivity of MWCNTs and PANI, and the decrease in carrier mobility was resulted from the strong interactions between MWCNTs and led to highest ε'' and tan δ_e.

4 Conclusions

MWCNTs/PANI nanocomposites with high absorbing properties were successfully synthesized. A possible formation mechanism of nanocomposites was proposed. The thermal stability and microwave absorbing properties of MWCNTs/PANI showed significant improvement. The reflection loss of MWCNTs/PANI was below −10 dB at 8.2–10.2 GHz, and the minimum loss value was −49.6 dB at 8.8 GHz, which was higher than that of single MWCNTs and pure PANI. The enhanced properties of MWCNTs/PANI were mainly due to the synergistic effect of MWCNTs and PANI. The excellent performances of obtained MWCNTs/PANI nanocomposites make them promising microwave absorbing materials.

References

1. J. Janata, M. Josowicz, Nat. Mat. **2**, 19 (2003)
2. M. Gerard, A. Chaubey, B.D. Malhotra, Biosens. Bioeletron. **17**, 345 (2002)
3. N.K. Guimard, N. Gomez, C.E. Schmidt, Prog. Polym. Sci. **32**, 876 (2007)
4. B. Guo, L. Glavas, A.-C. Albertsson, Prog. Polym. Sci. **38**, 1263 (2013)
5. G.A. Snook, P. Kao, A.S. Best, J. Power Sources **196**, 1 (2011)
6. L. Pan, H. Qiu, C. Dou, Y. Li, L. Pu, J. Xu, Y. Shi, Int. J. Mol. Sci. **11**, 2636 (2010)
7. A.K. Bakhshi, G. Bhalla, J. Sci. Ind. Res. **63**, 715 (2004)
8. Y. Wang, Int. J. Mater. Res. **105**, 3 (2014)
9. P.K. Khanna, N. Singh, S. Charan, A.K. Viswanath, Mater. Chem. Phys. **92**, 214 (2005)
10. S. Yang, X. Cui, J. Gong, Y. Deng, Chem. Commun. **49**, 4676 (2013)
11. F. Ahmed, S. Kumar, N. Arshi, M.S. Anwar, L. Su-Yeon, G.S. Kil, D.W. Park, B.H. Koo, C.G. Lee, Thin solid film **519**, 8375 (2011)
12. S. Radhakrishnan, C.R.K. Rao, M. Vijayan, J. Appl. Polym. Sci. **122**, 1510 (2011)
13. V. Mottaghitalab, G.M. Spinks, G.G. Wallace, Synth. Met. **152**, 77 (2005)
14. L. Nikzad, S. Alibeigi, M.R. Vaezi, B. Yazdani, M.R. Rahimi-pour, Chem. Eng. Technol. **32**, 861 (2009)
15. K.R. Reddy, B.C. Sin, K.S. Ryu, J. Noh, Y. Lee, Synth. Met. **159**, 1934 (2009)
16. Y. Meng, K. Wang, Y. Zhang, Z. Zhang, Adv. Mater. **25**, 6985 (2013)
17. H. Zengin, W. Zhou, J. Jin, R. Czerw, D.W. Smith Jr, L. Echegoyen, D.L. Carroll, S.H. Foulger, J. Ballato, Adv. Mater. **14**, 1480 (2002)
18. B. Yuan, L. Yu, L. Sheng, K. An, X. Zhao, J. Phys. D Appl. Phys. **45**, 235108 (2012)
19. A.L. Cabezas, X. Liu, Q. Chen, S.-L. Zhang, L.-R. Zheng, Z.-B. Zhang, Mater. **5**, 327 (2012)
20. L. Cui, J. Yu, Y. Lv, G. Li, S. Zhou, Polym. Compos. **34**, 1119 (2013)
21. S. Husain, S. Parveen, J. Ali, A. Kumar, M. Husain, Polym. Compos. **34**, 1298 (2013)
22. G. Chakraborty, K. Gupta, D. Rana, A.K. Meikap, Adv. Nat. Sci. Nanosci. Nanotechnol. **3**, 035015 (2012)
23. Z. He, S. Qi, X. Zhong, H. Qiu, J. Wang, J. Mater. Sci. Mater. Electron. **25**, 3455 (2014)
24. J. Xu, K. Wang, S.-Z. Zu, B.-H. Han, Z. Wei, ACS Nano **4**, 5019 (2010)
25. L. Wang, Y. Ye, X. Lu, Z. Wen, Z. Li, H. Hou, Y. Song, Sci. Rep. **3**, 3568 (2013)
26. H. Qiu, S. Qi, D. Wang, J. Wang, X. Wu, Synth. Met. **160**, 1179 (2010)
27. H. Qiu, S. Qi, J. Wang, D. Wang, X. Wu, Mater. Lett. **64**, 1964 (2010)
28. A. Liu, K. Sun, J. Yang, J. Nanopart. Res. **10**, 1303 (2008)

29. V. Gupta, T.A. Saleh, Synthesis of carbon nanotube-metal oxides composites; adsorption and photo-degradation, in *Carbon Nanotubes-From Research to Applications*, ed. by S. Bianco (InTech, Croatia, 2011), pp. 295–312
30. S.B. Kondawar, M.D. Deshpande, S.P. Agrawal, Int. J. Compos. Mater. **2**, 32 (2012)
31. J. Yu, N. Grossiord, C.E. Koning, J. Loos, Carbon **45**, 618 (2007)
32. S. Ding, H. Mao, W. Zhang, J. Appl. Polym. Sci. **109**, 2842 (2008)
33. T.H. Ting, Y.N. Jau, RPYu. Appl, Surf. Sci. **258**, 3184 (2012)
34. Y. Yang, S. Qi, Y. Qin, X. Zhang, J. Appl. Polym. Sci. **125**, 388 (2012)
35. T.K. Gupta, B.P. Singh, R.B. Mathur, S.R. Dhakate, Nanoscale **6**, 842 (2014)